

Railway track design & degradation

Mehran Sadri¹, Tao Lu¹, Arjen Zoeteman², and Michaël Steenbergen^{1,*}

¹Faculty of Civil Engineering and Geosciences, Delft University of Technology, Stevinweg 1, 2628 CN Delft, The Netherlands

²ProRail; Utrecht, The Netherlands

Abstract. The long-term behaviour of railway track has attracted increasing attention in recent years. Improvements in long-term structural performance reduce demands for maintenance and increase the continuous availability of railway lines. The focus of this paper is on the prediction of the sensitivity of a track design to long-term deterioration in terms of track geometry. According to the state of the art literature, degradation is often investigated using empirical models based on field measurement data. Although a rough maintenance forecast may be made employing empirical models, the predictions are not generic, and the physical processes which govern track degradation under train operation remain unclear. The first aim of this study is to present a mathematical model to elucidate the underlying physics of long-term degradation of railway tracks. The model consists of an infinitely long beam which is periodically supported by equidistantly discrete sleepers and a moving unsprung mass which represents a travelling train. The mechanical energy dissipated in the substructure is proposed to serve as a measure of the track degradation rate. Secondly, parametric studies on energy dissipation are conducted to identify effects of various track design parameters on the susceptibility of the track to degradation, as well as the effect of the train speed. It has been shown that the track/subgrade stiffness is the most influential parameter on degradation whereas other system parameters do influence the degradation rate but at lower magnitudes. The conclusions can be used to optimise the track design in the early stage for better long-term structural performance of railway tracks.

1 Mathematical formulation

To model the wheel/track interaction, the rail is represented by an infinite Timoshenko beam resting on equidistantly discrete supports of identical properties as shown in Fig. 1. EI , G and ρA are the bending stiffness, shear modulus and mass per unit length of the beam, respectively. κ is the shear coefficient of the cross section of the beam. For each support, the sleeper is modelled as a rigid mass M_s with l_s being the distance between neighbouring sleepers. The railpad that connects the sleeper and the rail is modelled as a spring-dashpot element with stiffness k_p and viscosity c_p , respectively. k_b and c_b represent the stiffness and the damping of the ballast. Moreover, the track is coupled to the unsprung wheel mass m_w moving at velocity v through a linearised contact spring of stiffness k_H .

*e-mail: M.J.M.M.Steenbergen@tudelft.nl

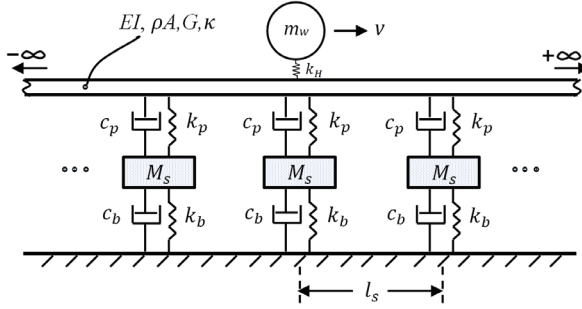


Figure 1. A moving wheel on a periodically supported beam [1].

Using the Timoshenko beam theory, the equations of motion for the rail can be written as:

$$\rho A \frac{\partial^2 w_b(x, t)}{\partial t^2} - \kappa A G \frac{\partial^2 w_b(x, t)}{\partial x^2} + \kappa A G \frac{\partial \psi_b(x, t)}{\partial x} = -F_c(t) \delta(x - vt) - \sum_{i=-N_s/2}^{N_s/2} R_i(t) \delta(x - il_s), \quad (1)$$

$$\rho I \frac{\partial^2 \psi_b(x, t)}{\partial t^2} - EI \frac{\partial^2 \psi_b(x, t)}{\partial x^2} - \kappa A G \frac{\partial w_b(x, t)}{\partial x} + \kappa A G \psi_b(x, t) = 0,$$

in which $\delta(\cdot)$ represents the Dirac-delta function. $w_b(x, t)$ and $\psi_b(x, t)$ denote the vertical displacement and the rotation angle of the beam, respectively. Due to the periodicity assumption, the following relationship can be established between the reaction force of the i th support, i.e. $R_i(t)$, and the reaction force of the 0th support $R_0(t)$,

$$R_i(t) = R_0(t - \frac{il_s}{v}). \quad (2)$$

The contact force $F_c(t)$ and reaction force of the 0th support $R_0(t)$ are defined in the following equations:

$$F_c(t) = k_H (w_b(vt, t) - w_w(t)), \quad (3)$$

$$R_0(t) = k_p \{w_b(0, t) - w_{s,0}(t)\} + c_p \{\dot{w}_b(0, t) - \dot{w}_{s,0}(t)\} \quad (4)$$

where $w_w(t)$ is the displacement of the wheel and $w_{s,0}(t)$ is the displacement of the middle sleeper at $x = 0$. Considering the interaction force between the rail and the 0th sleeper defined in Eq. (4), the equation of motion of the sleeper is

$$M_s \ddot{w}_{s,0}(t) = R_0(t) - c_b \dot{w}_{s,0}(t) - k_b w_{s,0}(t). \quad (5)$$

The equation of motion of the moving wheel can be written as follows,

$$m_w \ddot{w}_w(t) = k_H (w_b(vt, t) - w_w(t)) + m_{tot} g, \quad (6)$$

where $m_{tot}g$ is half the axle load. The following periodicity conditions are satisfied:

$$w_b(x + l_s, t + \frac{l_s}{v}) = w_b(x, t), \quad \psi_b(x + l_s, t + \frac{l_s}{v}) = \psi_b(x, t) \quad (7)$$

$$w_w(t + \frac{l_s}{v}) = w_w(t), \quad F_c(t + \frac{l_s}{v}) = F_c(t).$$

Therefore, the contact force can be expressed as a Fourier series,

$$F_c(t) = \sum_{m=-\infty}^{+\infty} \bar{F}_m e^{jm(\frac{2\pi v}{l_s})t} \quad (8)$$

where $j^2 = -1$ and \bar{F}_m are the unknown frequency-dependent coefficients of the contact force. Furthermore, Eq. (7) can be utilized in order to find a periodicity condition on the beam displacement and rotation, in the frequency domain,

$$\hat{w}_b(x, \omega) = e^{j\omega l_s/v} \hat{w}_b(x + l_s, \omega), \quad \hat{\psi}_b(x, \omega) = e^{j\omega l_s/v} \hat{\psi}_b(x + l_s, \omega). \quad (9)$$

Taking into consideration the latter relationships, it can be concluded that the displacement and rotation of the infinite beam are spatially periodic and they can consequently be expressed using the following Fourier series,

$$\hat{w}_b(x, \omega) = e^{-j\omega x/v} \sum_{m=-\infty}^{+\infty} \bar{W}_m(\omega) e^{jm(\frac{2\pi}{l_s})x}, \quad \hat{\psi}_b(x, \omega) = e^{-j\omega x/v} \sum_{m=-\infty}^{+\infty} \bar{\psi}_m(\omega) e^{jm(\frac{2\pi}{l_s})x}, \quad (10)$$

where $\bar{W}_m(\omega)$ and $\bar{\psi}_m(\omega)$ are the unknown frequency-dependent coefficients of the displacement and rotation responses. The responses of the rail, sleepers and the wheel can be solved in frequency domain. The time domain solution is obtained by inverse Fourier transform. For details of the solving procedure reference is made to [1].

2 Parametric study of track design and degradation

Degradation of track geometry is associated with non-elastic soil-ballast behaviour and energy dissipation in the substructure. Therefore, the latter is chosen as a measure for evaluating the long-term performance of railway track in service. A parametric study is conducted to illustrate the effect of various track design parameters on energy dissipation in the substructure. The nominal values of the wheel/track system are: (1) $EI = 4.25\text{MNm}^2$, $\rho A = 54.4\text{kgm}^{-1}$ and $\kappa = 0.34$ for the rail; (2) $M_s = 142.5\text{kg}$ for sleepers and the distance between sleepers $l_s = 0.6\text{m}$; (3) $k_p = 1000\text{MNm}^{-1}$ and $c_p = 30\text{kNm}^{-1}\text{s}$ for railpads; (4) $k_b = 50\text{MNm}^{-1}$ and $c_b = 55\text{kNm}^{-1}\text{s}$ for ballast; (5) $m_w = 900\text{kg}$ for the wheel mass and the linearised contact stiffness $k_H = \sqrt[3]{3 \times 10^{22} \cdot Q}$ where $Q = 100\text{kN}$ is the static wheel load. These values correspond to typical Dutch railway track [1, 2].

2.1 Mechanical energy dissipation in the substructure

The mechanical energy dissipated in the substructure, for a single passage of the moving wheel, and for the position at the 0th support is given by:

$$E_{diss,0} = \int_{-\infty}^{+\infty} c_b v_{s,0}(t)^2 dt \quad (11)$$

where $v_{s,0}(t)$ is the time domain velocity of the sleeper at $x = 0$.

2.2 Receptance of an individual sleeper

Before proceeding to the parametric study, the wheel/track receptance is examined. The receptance is widely used in the literature to demonstrate the properties of railway tracks e.g.

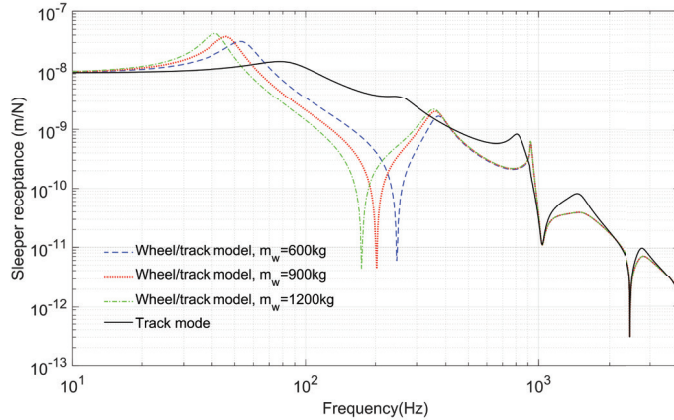


Figure 2. Receptance of an individual sleeper.

[3–5]. Since the dissipated energy is associated with the response of the sleeper as shown in Eq. (11), therefore, the receptance of an individual sleeper under stationary harmonic load and wheel both positioned on the rail above a sleeper is shown in Fig. 2. The way the receptance is calculated is described in [1]. Three different unsprung wheel mass values are used to show its importance on the frequency response of the sleeper. Nominal values of other track parameters given previously are adopted. The unsprung mass causes a significant decrease of the first and second resonant frequencies.

2.3 Effects of ballast and railpad properties

The ballast/soil properties play an important role in the energy dissipation in the subgrade. Fig. 3(a) shows the effect of ballast stiffness on dissipated energy. Generally, the higher the

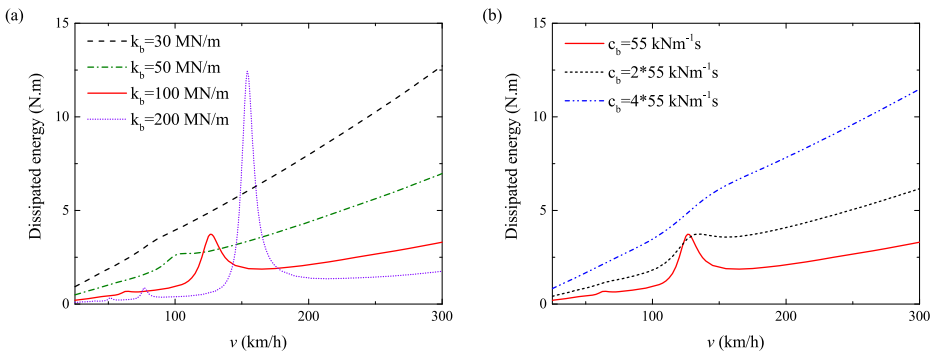


Figure 3. Effects of ballast/subgrade properties on the dissipated energy: (a) $c_b = 55\text{kNm}^{-1}\text{s}$; (b) $k_b = 100\text{MNm}^{-1}$. Nominal values for other parameters.

track stiffness, the lower the dissipated energy. However, for higher track stiffness, dissipation peaks appear at specific speeds. At these speeds, the sleeper passing frequency v/l_s or its multiples coincide with the first resonant frequency in the system receptance in Fig. 2 [1].

The speeds at which peak values of dissipated energy occur are of practical importance since they fall into the operational speed range of conventional trains. In Fig. 3(b), the track stiffness is fixed to $k_b = 100\text{MNm}^{-1}$ and the effect of ballast damping on dissipated energy is investigated. As expected, higher damping results in a higher dissipated energy level in absolute sense. However, it becomes also clear that the magnitude of the dissipation peaks is influenced significantly by the damping value; also the speed corresponding to these peaks shifts upward.

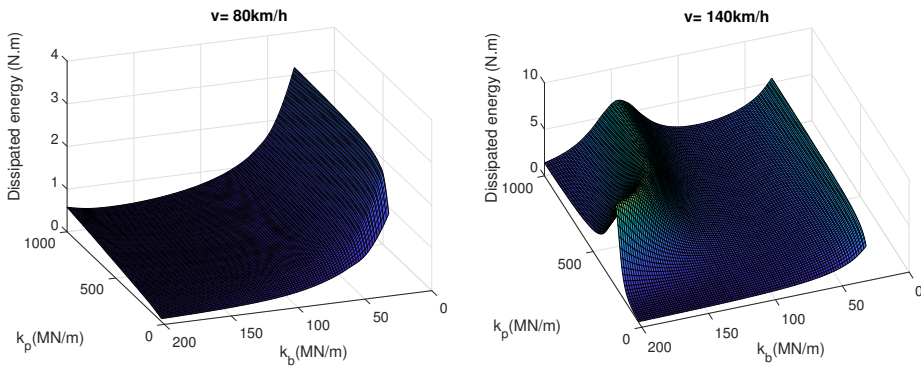


Figure 4. 3D plot of dissipated energy for ballast stiffness range $30 - 200\text{MNm}^{-1}$ and railpad stiffness range $30 - 1000\text{MNm}^{-1}$ for speed: $v = 80\text{km/h}$ on the left; $v = 140\text{km/h}$ on the right.

3D plots of dissipated energy level for different combinations of ballast and railpad stiffness are shown in Fig. 4 for two typical operational speeds of conventional trains: freight and passenger trains. At $v = 80\text{km/h}$, for a specific k_b , the dissipated energy (and therefore the expected degradation) grows with increasing railpad stiffness. In contrast, energy dissipation decreases with higher track stiffness. The effect of the track stiffness exceeds that of the railpad stiffness. At speed $v = 140\text{km/h}$, the situation is more complicated, due to the fact that

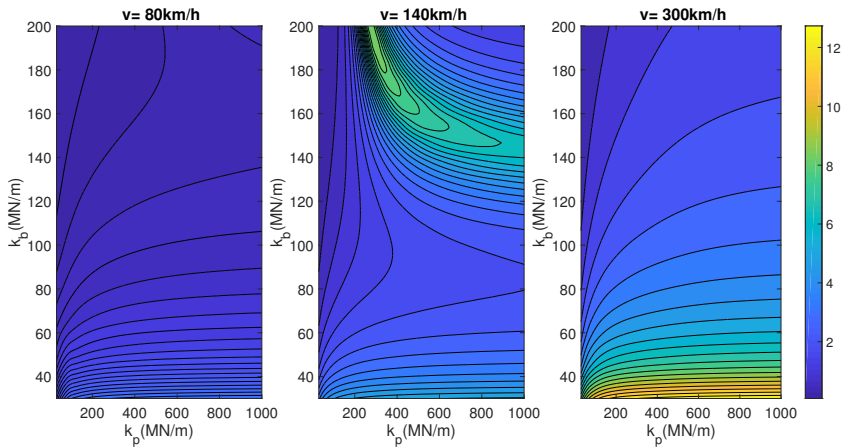


Figure 5. Contour plot of dissipated energy (unit N.m) for ballast stiffness range $30 - 200\text{MNm}^{-1}$ and railpad stiffness range $30 - 1000\text{MNm}^{-1}$.

this speed falls into the range where peak energy dissipation may occur as shown in Fig. 3. Low track stiffness, roughly below 70MN/m is always unfavourable. A track stiffness around 100 MN/m can be seen to minimise energy dissipation independent of the railpad stiffness. For higher track stiffness, the magnitude of the railpad stiffness starts to play a significant role and therefore clearly needs optimisation.

The possibilities of the developed methodology are illustrated in Fig. 5, showing a contour plot of the dissipated energy in the substructure, as a function of both track stiffness and railpad stiffness, for three different train speeds. The system parameter combination zones with the lowest energy dissipation for any train speed combination can be easily identified. These kind of maps can be plotted for any parameter combination, allowing for an optimised track design under specific conditions.

2.4 Effects of other parameters

In the previous, parameters such as the wheel mass, the distance between neighbouring sleepers, mass of the sleepers, railpad damping and rail cross-sectional profile were not discussed. Apart from the rail profile, they play less significant roles with respect to the expected degradation [1]. Higher unsprung mass decreases the speed with peak energy dissipation. This is because larger wheel mass moves the first resonant frequency of the sleeper receptance to a lower value as shown in Fig. 2. Decreasing sleeper distance leads to lower energy dissipation, but on the other hand adapting this distance is often not a feasible option. The dissipated energy decreases for a stiffer rail profile. The railpad damping and the sleeper mass have very limited effect on the dissipated energy in the substructure for typical Dutch railway track.

3 Conclusions

In this paper, a two-layer frequency-domain track model is employed to deal with wheel/track interaction. The focus is placed on the mechanical energy dissipated in the substructure, which is proposed to serve as a measure of the expected track degradation. Effects of various wheel/track parameters on energy dissipation are investigated, as well as the effect of the train speed. The nominal values of these parameters are from Dutch railway practice. The most important system parameter is the track/subgrade stiffness. The degradation increases with the train speed and with softer subgrade in general. However, stiff subgrades appear more sensitive to particular train velocities (100-200km/h) since the energy dissipation may have peak values. Larger subgrade damping attenuates these peaks and shifts them to a larger speed. It is also concluded that increasing railpad stiffness causes higher degradation rates. Therefore, a combination of low railpad stiffness and high track stiffness is preferred in many cases of track design. Larger sleeper distance also increases dissipated energy. In contrast, application of a stiffer rail profile decreases the degradation rate. Unsprung vehicle mass and sleeper mass have very limited influence on geometrically perfect tracks with a uniform stiffness profile (apart from the discrete supports) considered in this paper.

References

- [1] M. Sadri, M. Steenbergen, J. Sound Vib. **419**, 271 (2018)
- [2] C. Esveld, *Modern Railway Track* (MRT-productions Zaltbommel, The Netherlands, 2001)
- [3] T. Wu, D.J. Thompson, J. Sound Vib. **219**, 881 (1999)
- [4] T. Mazilu, J. Sound Vib. **306**, 31 (2007)
- [5] K. Knothe, Y. Wu, Arch. Appl. Mech. **68**, 457 (1998)